Octupole electrode pattern for tuning forks vibrating at the first overtone mode in quartz-enhanced photoacoustic spectroscopy

A. Elefante[a], P. Patimisco[a], A. Sampaolo[a], M. Giglio[a], G. Menduni[a,b], H. Rossmadl[c], V. Mackowiak[c], V. Passaro[b], Bruno Gross[d], Alex Cable[d], F. K. Tittel[e], and V. Spagnolo[a]

[a] PolySense Lab - Dipartimento Interateneo di Fisica, University and Politecnico of Bari, Via Amendola 173, Bari, Italy
[b]Photonics Research Group, Dipartimento di Ingegneria Elettrica e dell'informazione, Politecnico di Bari, Via Orabona 4, Bari, 70126, Italy
[c]Thorlabs GmbH, Hans-Boeckler-Straße 6, 85221 Dachau, Germany
[d]Thorlabs, Inc., 56 Sparta Ave., Newton, 07860, USA
[e]Department of Electrical and Computer Engineering, Rice University, 6100 Main Street, Houston, TX 77005, USA

ABSTRACT

We report on a comparison between two quartz tuning forks (QTFs) employed for quartz-enhanced photoacoustic spectroscopy (QEPAS) having quadrupole and octupole electrode pattern configurations. With respect to the quadrupole, the implementation of the octupole pattern suppresses the fundamental mode and reduces by a factor of ~ 4.4 the electrical resistance for the first overtone mode with negligible variations of the related Q-factors. Both QTFs operating at the first overtone mode were implemented in a QEPAS sensor and the results showed that the octupole configuration provides a ~2.3 signal enhancement factor.

Keywords: quartz-enhanced photoacoustic spectroscopy, gas sensing, tuning fork, overtone mode, octupole.

1. INTRODUCTION

Quartz tuning forks (QTFs) represent the core of the quartz-enhanced photoacoustic spectroscopy (QEPAS) for gas traces detection [1-10]. The feasibility to realize custom-made QTFs optimized for sensing applications can significantly improve the performance of QEPAS sensors [11-20]. With respect to the standard 32.7 kHz-QTF, the resonance frequency of the fundamental mode can be reduced to a few kHz in order to better approach the typical energy relaxation time of targeted gases [21-22] while maintaining a high resonator quality factor. Both conditions can be simultaneously satisfied by an appropriate design of the QTF prong sizes. However, lowering the fundamental resonance frequency reduces also the first overtone mode frequencies, opening the way to their investigation and implementation in QEPAS sensor systems [13, 18]. This was not feasible with a 32.7 kHz-QTF since its first overtone mode occurs at frequencies higher than 190 kHz, which is impractical for QEPAS based gas detection. By using the Euler-Bernoulli equation the first overtone mode exhibits a resonance frequency ~ 6.3 times higher than the fundamental mode [23]. This implies that in order to have the first overtone resonance frequency < 30 kHz, the fundamental mode must fall at frequencies lower than 4.5 kHz. Lowering the operating frequency at values below 3 kHz is not recommended for QEPAS since the sensor system would be more influenced by environmental acoustic noise. The fundamental and the first overtone modes exhibit different quality factor values because the associated loss mechanisms depend on the related vibrational dynamics and on the geometry of the QTF prongs [24]. Hence, the QTF geometry can be designed to provide an enhancement of the overtone mode resonance Q-factor. As a consequence, a higher QEPAS signal-to-noise ratio with respect to the fundamental mode can be expected [18]. According to Hosaka's model [25] the air damping is significantly reduced when moving from the fundamental to overtone mode. However, if moving to higher modes, support losses can start to dominate deteriorating the overall quality factor. An increase of a factor of ~ 12 on support losses is expected for a QTF, when changing from the fundamental to the first overtone mode [26]. The quality factor of

Quantum Sensing and Nano Electronics and Photonics XVI, edited by Manijeh Razeghi, Jay S. Lewis, Eric Tournié, Giti A. Khodaparast, Proc. of SPIE Vol. 10926, 109262K

the first overtone mode can be higher than that of the fundamental one, which is beneficial for QEPAS performance, even if these QTFs employed a quadrupole configuration of the electrode pattern. Indeed, the quadrupole layout is designed to match the charge distribution generated by the in-plane fundamental mode vibration. Nevertheless, it has shown that the first overtone mode can be also excited, even if such an electrode configuration partially impedes the excitation of the first overtone flexural mode [27].

In this work, we realized two QTFs, QTF-Q and QTF-O, having the same size, but different contact pattern layouts to study their influence on the QTF electrical properties and sensing performance. The QTF-Q has a standard quadrupole electrode configuration, while the QTF-O has an innovative octupole layout, designed to optimize the first overtone flexural mode charge collection. By investigating the electrical properties of both QTFs, we demonstrated that the octupole configuration completely suppresses the fundamental one. As expected, both QTFs exhibits almost the same Q-factor value for the first overtone mode (<5% difference) since Q-factor values should be independent from the contact pattern configuration. The octupole configuration allows the reduction of the electrical resistance by a factor of ~4.4 with respect to the QTF-Q. Both QTFs were tested in a mid-IR QEPAS sensor targeting a water absorption line located at 1931.76 cm^{-1}. We verified that the larger electrical conductance of the QTF-O provides improved performance for gas sensing, resulting in a QEPAS signal ~2.3 times higher than the QTF-Q.

2. OCTUPOLE ELECTRODE LAYOUT

For a QTF vibrating in its in-plane flexural modes, the prong dynamics in a direction perpendicular to the prong at the rest position can be described by the Euler-Bernoulli (E-B) equation [23]. The E-B equation can be solved by imposing clamped-free boundary conditions, assuming that one prong end is fixed and the other one is free to oscillate at its natural frequency. The analytic solution for the flexural vibration resonance frequencies is given by:

$$f_n = \frac{\pi T}{8\sqrt{12}L^2}\sqrt{\frac{E}{\rho}}\upsilon_n^2 \tag{1}$$

where E = 0.72·1011 N/m^2 and ρ = 2650 Kg/m^3 denote the Young's modulus and the density of quartz, respectively, T and L are the prong thickness and length, respectively, and n identifies the mode number (υ_1 = 1.194 for the fundamental mode and υ_2 = 2.988 for the first overtone mode). The E-B equation predicts also the lateral displacement of the prong vibrating at one of its natural modes as a function of the distance from the prong base [18]:

$$y(x) \propto \left[\cos(k_n x) - \cosh(k_n x)\right] + \left[\frac{-\cos(k_n L) - \cosh(k_n L)}{\sin(k_n L) - \sinh(k_n L)}\right]\left[\sin(k_n x) - \sinh(k_n x)\right] \tag{2}$$

where $k_n \cdot L$ are constant values related to the resonance frequencies for the vibrating prong: $k_1 L$ = 1.875 for the fundamental mode and $k_2 L$ = 4.694 for the first overtone mode. The normalized lateral displacements of the prong having a length of 17 mm as a function of the distance from the prong base for the fundamental and first overtone mode are shown in Fig. 1.

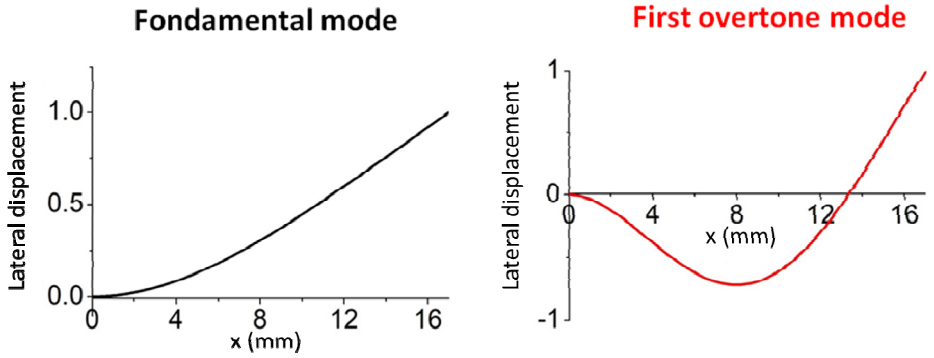

Figure 1. Lateral displacement along the QTF prong as a function of the distance from the prong-support junction for the fundamental (black solid lines) and the first overtone (red solid lines) mode. The prong length is L = 17 mm.

An innovative electrode pattern optimizing the first overtone flexural mode charge collection must follow the stress field distribution along the QTF prongs. When the prongs of a tuning fork are in their natural oscillatory motion, the stress produced along the prong can be expressed by a longitudinal tensor $\sigma_p(x,z)$, where x and y identify a Cartesian plane orthogonal to the prong. The stress induces a local polarization $p_0(x,y)$ of quartz and charges appearing on the surface can be collected by electrical contacts deposited along the QTF prong. The polarization depends on the stress field as $p_0 = [d]\sigma_p$, where [d] is the quartz piezoelectric tensor. Assuming that the QTF axes correspond to the quartz crystal axes and considering the effects of the polarization perpendicular to the tensile stress, the relation between p_0 and σ_p reduces to the scalar expression $p_0 = -d_{11}\sigma_p$, where d_{11} is the longitudinal piezoelectric modulus. In the elastic regime, in which there is a linear relationship between the stress and strain fields, it can be shown that σ_p is proportional to the second derivative of the displacement for a bent QTF prong [27]. By using Eq. (2), the tensile stress along the prong axis is given by:

$$\sigma_p(x) \propto \left[-\cosh(k_n x) - \cos(k_n x)\right] + \left[\frac{-\cos(k_n L) - \cosh(k_n L)}{\sin(k_n L) - \sinh(k_n L)}\right]\left[-\sinh(k_n x) - \sin(k_n x)\right] \quad (3)$$

The curves in Fig. 2 show the distribution of normalized strain along the prong as a function of the distance from the prong base for the fundamental and first overtone mode obtained by using Eq. (3) with L = 17 mm.

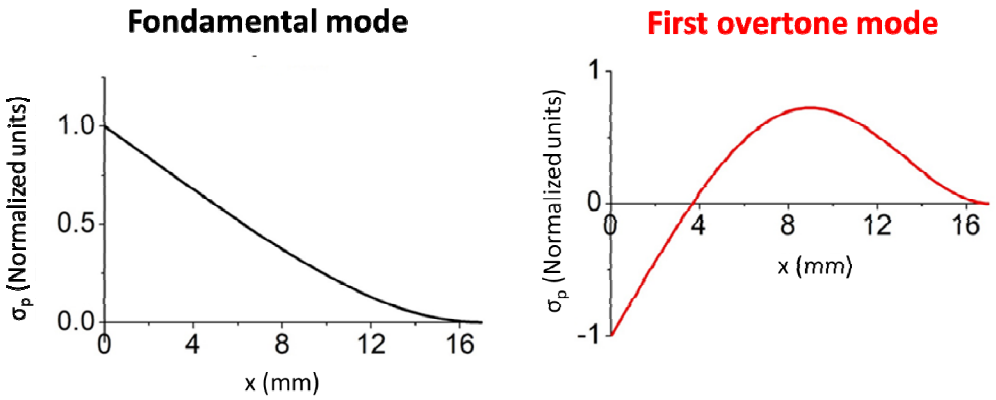

Figure 2. One-dimensional normalized stress field distribution along the QTF prong as a function of the distance from the prong base for the fundamental (black solid lines) and the first overtone (red solid lines) mode. The prong length is L = 17 mm.

The fundamental mode shows the highest stress antinode at x = 0. The first overtone mode shows two stress antinode points, one negative at x = 0 and one positive at x = 9 mm. For the fundamental vibrational mode, the sign of the strain distribution does not change over the entire length of the QTF prong. However, for the first overtone mode the strain direction changes along the length of the prong and consequently also the sign of the piezoelectrically induced charges, which reverses at the zero-stress point. The electrode patterns deposited on QTF surfaces must be divided into separated zones corresponding to opposite generated electric fields (and charges) areas in order to efficiently retrieve the piezoelectric signal provided by a specific flexural resonance mode. The separation between electrodes of different polarity is located where the sign of the strain field reverses. For the fundamental flexural mode, the sign of the stress (and thereby of the generated charges) alternates between adjacent lateral prong surfaces but remains the same along the prong length. Hence, a quadrupole electrode pattern should be employed. Furthermore, for the overtone mode the sign of the stress is opposite over adjacent surfaces. Nevertheless, the electrode pattern must be sectioned along the prong surface due to the presence of a zero-stress point, delimiting areas characterized by opposite stress signs and generated charges. This requires a dual-quadrupole electrode layout configuration, i.e. an octupole electrode pattern for optimal charge collection. The octupole electrode pattern was designed and realized for a QTF having: prongs length and width of L = 17 mm and w = 1.0 mm, respectively, starting from a quartz crystal with a thickness of 0.25 mm. In Fig. 3, a sketch of the QTF with the octupole electrode layout (QTF-O) is shown.

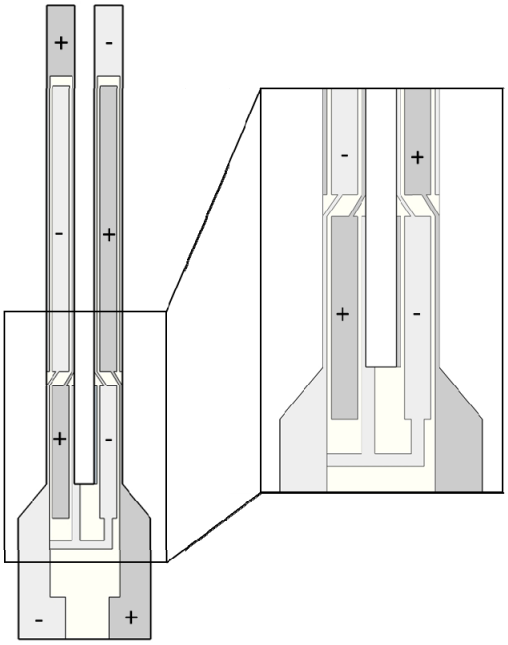

Figure 3. Schematic of the QTF-O having an octupole electrode pattern. A zoom of the area in which the electrode polarity is inverted is shown on the right side.

According to Fig. 2, a zero-stress point along the prong occurs at 3.8 mm from the prong base. At such a point, the electrode polarity has been inverted.

3. CHARACTERIZATION OF THE Q-QTF

In order to study the influence of the electrode layout on the QTF performance, a QTF having the same prong sizes (L = 17 mm and w = 1.0 mm, with a crystal thickness of 0.25 mm) of the QTF-O, but with a standard quadrupole electrode configuration (QTF-Q), was realized. The electrical characterization of the QTF-Q and the QTF-O was performed by exciting the resonator electrically. A sinusoidal voltage excitation generates a charge displacement through the QTF prongs. The piezoelectric current is then converted to an output voltage by means of the trans-impedance amplifier and then the lock-in amplifier demodulates the signal at the same frequency as the waveform generator. The spectral response was fitted using a Lorentzian function to determine the peak resonance frequency and the full-width-half-maximum value: the ratio between these two values allows the estimation of the quality factor. In Fig. 4, the resonance curves for the first overtone flexural mode are shown for the QTF-O and the QTF-Q at atmospheric pressure. The resonance frequencies, the quality factors and the electrical resistances are also reported, extracted from both resonance curves.

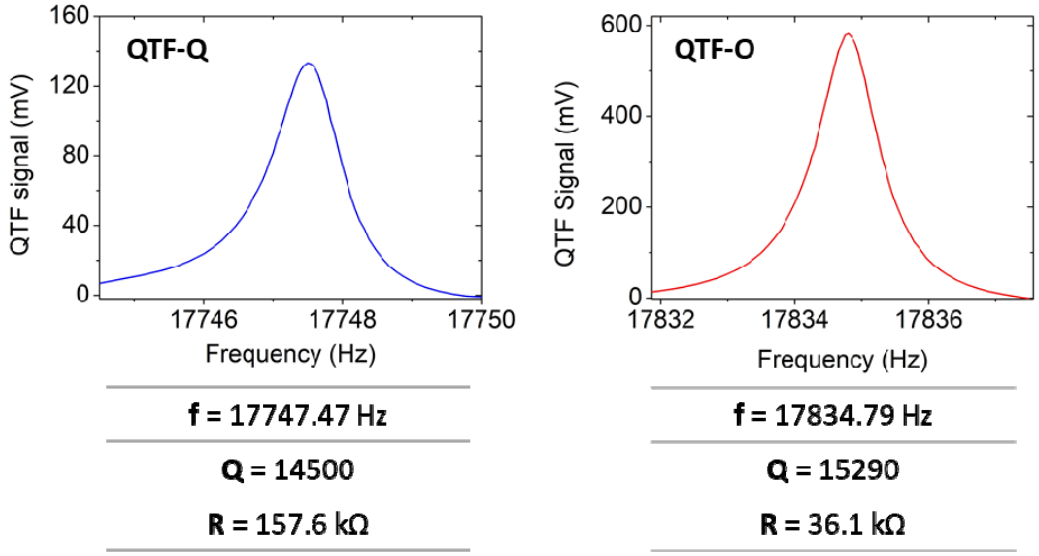

Figure 4. Resonance curves measured at a fixed excitation level V = 300 mV and at atmospheric pressure for the QTF-Q (blue solid line) and the QTF-O (red solid line).

The resonance frequency as well as the Q-factor of the first overtone mode are affected by the electrode pattern. This is to be expected because the resonance frequency is determined by the material and the geometry of the prong (see Eq. 1), and the quality factor is mainly affected by loss mechanisms occurring in the vibrating prongs (due to interaction with the surrounding fluid and with the fixed support) and not by the charge collection efficiency [25-26]. The effect of the octupole contact pattern is to reduce the electrical resistance by a factor of ~ 4.4, demonstrating an increase of the piezoelectric charge efficiency collection when the octupole electrode pattern is employed for the first overtone mode. To verify if the reduction of the electrical resistance is beneficial for QEPAS sensing, both QTFs were implemented in a QEPAS setup, similar to that reported in Ref. [27]. A continuous-wave quantum cascade laser (QCL) was used as light source to generate photoacoustic signals when a water vapor absorption line located at 1931.76 cm^{-1} (line-strength of $3.2 \cdot 10^{-22}$ cm/molecule) was excited. An aluminum housing filled with standard air at a fixed 1.7% water vapor concentration at atmospheric was realized to accommodate and easily exchange the two QTFs. The sensor operated in wavelength modulation and dual-frequency detection: the laser current was modulated at half of the QTF resonance frequency and the QTF signal demodulated at the QTF resonance frequency. With this approach, while the laser current is scanned across the selected water absorption line, the QEPAS signal resembles a second derivative of the Lorentzian lineshape of the absorption line, with a small contribution due to the residual amplitude modulation [28-29]. The QEPAS spectral scans of the selected water absorption line obtained for the QTF-O and the QTF-Q while vibrating at the first overtone mode are shown in Fig. 5.

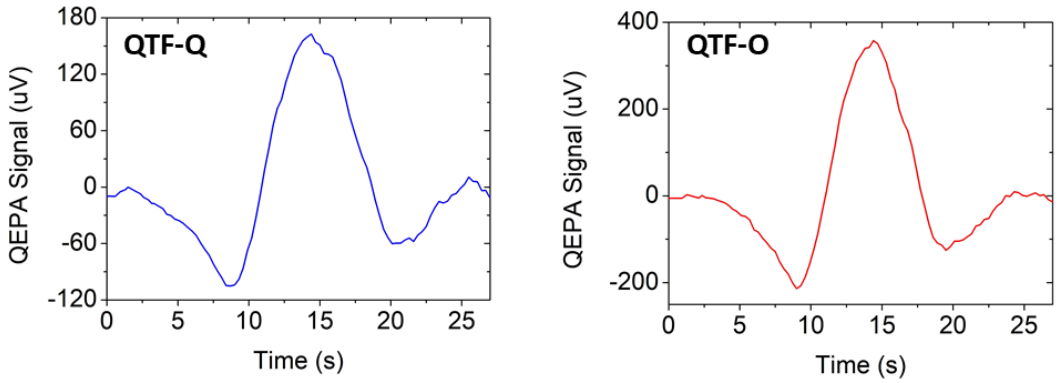

Figure 5. QEPAS spectral scans of the water absorption line measured with the QTF-Q (solid blue curve) and the QTF-Q (solid red curve) operating at the first overtone mode.

The QEPAS spectra show that the peak value measured for QTF-O (357.8 μV) operating at the overtone mode is ~2.3 times higher than that obtained with QTF-Q (155.6 μV) operating at the overtone mode.

4. Q-QTF COUPLED WITH A DUAL-TUBE RESONATOR SYSTEM

The Q-QTF was acoustically coupled with a pair of micro-resonator tubes, acting as amplifiers for the sound wave. The system composed by a QTF and resonator tubes is usually referred as a spectrophone. The QTF-Q was positioned between the tubes to probe the acoustic vibration excited in the absorbing gas contained inside the tubes. The geometrical parameters influencing the sensor performance are: the internal diameter ID and the length *l* of the two tubes, together with the spacing between the tube and the surface of the QTF [30]. By using guidelines provided in Ref. [2], two tubes with an ID = 1.27 mm having a length of *l* =7.0 mm (outer diameter of 1.47 mm), both located 200 μm from the QTF prong surface were selected. With such a spectrophone, the QEPAS scan of the water absorption line is shown in Fig. 6, together with a resonance curve.

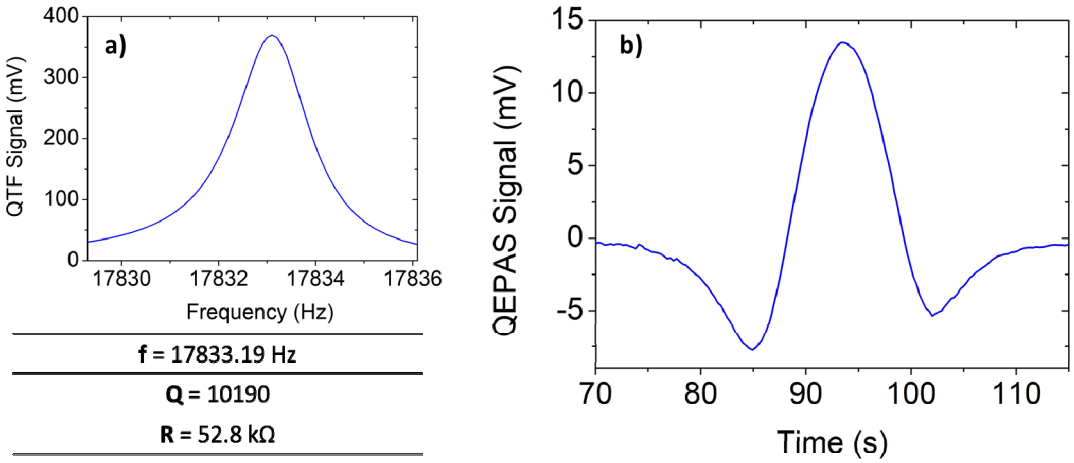

Figure 6. (a) Resonance curve measured at a fixed excitation level V = 300 mV and at atmospheric pressure with the spectrophone composed of the QTF-Q and a pair of micro-resonator tubes having a length of 7.0 mm and internal diameter of 1.27 mm, both positioned 200 μm from the QTF. (b) QEPAS spectral scan acquired with the same spectrophone.

The acoustic coupling reduced the resonance frequency of the QTF of 1.6 Hz and the quality factor of 33.3%. However, taking advantage from the sound wave enhancement produced by the microresonator tubes, the QEPAS peak signal reached 13.46 mV, ~38 times higher than that measured with the bare QTF-Q.

5. CONCLUSIONS

In this work, we demonstrated that an octupole electrode pattern configuration for a QTF vibrating at the first overtone mode lowers the electrical resistance with respect to the quadrupole electrode pattern. This provides higher signals when implemented in a QEPAS sensor system. We demonstrated an enhancement of the QEPAS signal of factor of 2.3 with respect to the quadrupole pattern configuration. When coupled with a dual-microresonator tubes system, the QEPAS signal is further enhanced by a factor of 38.

6. AKNOWLEDGMENTS

The authors from Dipartimento Interateneo di Fisica di Bari acknowledge financial support from THORLABS GmbH, within the joint research laboratory PolySense. Frank K. Tittel acknowledges support by the Welch Foundation under Grant No. C0568.

REFERENCES

[1] Patimisco, P., Scamarcio, G., Tittel, F.K., Spagnolo, V., "Quartz-Enhanced Photoacoustic Spectroscopy: A Review," Sensors 14, 6165-6206 (2014).

[2] Patimisco, P., Sampaolo, A., Zheng, H., Dong, L., Tittel, F.K. and Spagnolo V., "Quartz enhanced photoacoustic spectrophones exploiting custom tuning forks: a review," Adv. Phys. X 2, 169-187 (2016).

[3] Patimisco, P., Sampaolo, A., Dong, L., Tittel, F.K., Spagnolo V., "Recent advances in quartz enhanced photoacoustic sensing," Appl. Phys. Rev., 011106 (2018).

[4] Jahjah, M., Jiang, W., Sanchez, N.P., Ren, W., Patimisco, P., Spagnolo, V., Herndon, S.C., Griffin, R.J., and Tittel, F.K., "Atmospheric CH_4 and N_2O measurements near Greater Houston area landfills using QCL-based QEPAS sensor system during DISCOVERY-AQ 2013," Opt. Lett. 39, 957-960 (2014).

[5] Sampaolo, A., Patimisco, P., Giglio, M., Chieco, L., Scamarcio, G., Tittel, F.K., and Spagnolo, V., "Highly sensitive gas leak detector based on a quartz-enhanced photoacoustic SF_6 sensor," Opt. Express 24, 15872-15881 (2016).

[6] Patimisco, P., Spagnolo, V., Vitiello, M. S., Tredicucci, A., Scamarcio, G., Bledt, C. M., and Harrington, J. A., "Coupling external cavity mid-IR quantum cascade lasers with low loss hollow metallic/dielectric waveguides," Appl. Phys. B 108, 255–260 (2012).

[7] Viciani, S., Siciliani de Cumis, M., Borri, S., Patimisco, P., Sampaolo, A., Scamarcio, G., De Natale, P., D'Amato, F., and Spagnolo, V., "A quartz-enhanced photoacoustic sensor for H2S trace-gas detection at 2.6 μm," Appl. Phys. B 119, 21-27 (2014).

[8] Giglio, M., Patimisco, P., Sampaolo, A., Scamarcio, G., Tittel, F. K., and Spagnolo, V., "Allan Deviation Plot as a Tool for Quartz-Enhanced Photoacoustic Sensors Noise Analysis," IEEE Trans. Ultrason. Ferroelect. Freq. Control, 63, 555-560 (2016).

[9] Wang, Q., Wang, Z., Ren, W., Patimisco, P., Sampaolo, A., and Spagnolo, V., "Fiber-ring laser intracavity QEPAS gas sensor using a 7.2 kHz quartz tuning fork," Sensor Actuat. B-Chem. 227268, 512-518 (2018).

[10] Wu, H., Sampaolo, A., Dong, L., Patimisco, P., Liu, X., Zheng, H., Yin, X., Ma, W., Zhang, L., Yin, W., Spagnolo, V., Jia, S., and Tittel, F.K., "Quartz enhanced photoacoustic H_2S gas sensor based on a fiber-amplifier source and a custom tuning fork with large prong spacing," Appl. Phys. Lett. 107, 111104 (2015).

[11] Sampaolo, A., Patimisco, P., Giglio, M., Vitiello, M.S., Beere, H.E., Ritchie. D.A., Scamarcio, G., Tittel, F. K., and Spagnolo, V., "Improved Tuning Fork for Terahertz Quartz-Enhanced Photoacoustic Spectroscopy," Sensors, 16, 439 (2016).

[12] Spagnolo, V., Patimisco, P., Pennetta, R., Sampaolo, A., Scamarcio, G., Vitiello, M.S., Tittel, F.K., "THz Quartz-enhanced photoacoustic sensor for H_2S trace gas detection," Opt. Express 23, 7574-7582 (2015).

[13] Sampaolo, A., Patimisco, P., Dong, L., Geras, A., Scamarcio, G., Starecki, T., Tittel, F. K., and Spagnolo, V., "Quartz-enhanced photoacoustic spectroscopy exploiting tuning fork overtone modes," Appl. Phys. Lett. 107, 231102 (2015).

[14] Zheng, H., Dong, L., Sampaolo, A., Wu, H., Patimisco, P., Yin, X., Ma, W., Zhang, L., Yin, W., Spagnolo, V., Jia, S., Tittel, F.K., "Single-tube on-beam quartz-enhanced photoacoustic spectroscopy," Opt. Lett. 41, 978-981 (2016).

[15] Zheng, H., Dong, L., Patimisco, P., Wu, H., Sampaolo, A., Yin, X., Li, S., Ma, W., Zhang, L., Yin, W., Xiao, L., Spagnolo, V., Jia, S., Tittel, F.K., "Double antinode excited quartz-enhanced photoacoustic spectrophone," Appl. Phys. Lett. 110, 021110 (2017).

[16] Wu, H., Yin, X., Dong, L., Pei, K., Sampaolo, A., Patimisco, P., Zheng, H., Ma, W., Zhang, L., Yin, W., Xiao, L., Spagnolo, V., Jia, S., Tittel, F.K., "Simultaneous dual-gas QEPAS detection based on a fundamental and overtone combined vibration of quartz tuning fork," Appl. Phys. Lett. 110, 121104 (2017).

[17] Zheng, H., Dong, L., Sampaolo, A., Wu, H., Patimisco, P., Ma, W., Zhang, L., Yin, W., Xiao, L., Spagnolo, V., Jia, S., and Tittel, F.K., "Overtone resonance enhanced single-tube on-beam quartz enhanced photoacoustic spectrophone," Appl. Phys. Lett. 109, 111103 (2016).

[18] Tittel, F.K., Sampaolo, A., Patimisco, P., Dong, L., Geras, A., Starecki, T., and Spagnolo, V., "Analysis of overtone flexural modes operation in quartz-enhanced photoacoustic spectroscopy," Opt. Express 24, A682-A692 (2016).

[19] Patimisco, P., Sampaolo, A., Dong, L., Giglio, M., Scamarcio, G., Tittel, F.K., and Spagnolo, V., "Analysis of the electro-elastic properties of custom quartz tuning forks for optoacoustic gas sensing," Sensor Actuat. B-Chem. 227, 539-546 (2016).

[20] Giglio, M., Patimisco, P., Sampaolo, A., Zifarelli, A., Blanchard, R., Pfluegl, C., Witinski, M.F., Vakhshoori, D., Tittel, F.K., and Spagnolo, V., Nitrous oxide quartz-enhanced photoacoustic detection employing a broadband distributed-feedback quantum cascade laser array," Appl. Phys. Lett. 113, 171101 (2018).
[21] Wysocki, G., Kosterev, A.A., and Tittel, F.K., "Influence of molecular relaxation dynamics on quartz-enhanced photoacoustic detection of CO_2 at $\lambda = 2$ μm," Appl. Phys. B 85, 301-306 (2006).
[22] Kosterev, A.A., Mosely, T.S., and Tittel, F.K., "Impact of humidity on quartz-enhanced photoacoustic spectroscopy based detection of HCN," Appl. Phys. B 85, 295–300 (2006).
[23] Patimisco, P., Borri, S., Sampaolo, A., Beere, H.E., Ritchie, D.A., Vitiello, M.S., Scamarcio, G., and Spagnolo, V., "Quartz enhanced photo-acoustic gas sensor based on custom tuning fork and terahertz quantum cascade laser," Analyst 139, 2079-2087 (2014).
[24] Patimisco, P., Sampaolo, A., Mackowiak, V., Rossmadl, H., Cable, A., Tittel, F.K., and Spagnolo, V., "Loss Mechanisms Determining the Quality Factors in Quartz Tuning Forks Vibrating at the Fundamental and First Overtone Modes," IEEE Trans. Ultrason. Ferroelect. Freq. Control 65, 1951-1957 (2018).
[25] Hosaka, H., Itao, K., Kuroda, S., "Damping characteristics of beam-shaped micro-oscillators," Sensor. Actuat. A-Phys. 49, 87-95, 1995.
[26] Hao, Z., Erbil, A., Ayazi, F., "An analytical model for support loss in micromachined beam resonators with in-plane flexural vibrations. Sensor," Actuat. A-Phys. 109, 156-164, 2003.
[27] Patimisco, P., Sampaolo, A., Giglio, M., Mackoviak, V., Rossmadl, H., Gross, B., Cable, A., Tittel, F.K., and Spagnolo, V., "Octupole electrode pattern for tuning forks vibrating at the first overtone mode in quartz-enhanced photoacoustic spectroscopy," Opt. Lett. 43, 1854-1857 (2018).
[28] Bidaux, Y., Bismuto, A., Patimisco, P., Sampaolo, A., Gresch, T., Strubi, G., Blaser, S., Tittel, F.K., Spagnolo, V., Muller, A., and Faist, J., "Mid infrared quantum cascade laser operating in pure amplitude modulation for background-free trace gas spectroscopy," Opt. Express 24, 26464-26471 (2016).
[29] Patimisco, P., Sampaolo, A., Bidaux, Y., Bismuto, A., Schott, M., Jiang, J., Muller, A., Faist, J., Tittel, F.K., and Spagnolo, V., "Purely wavelength- and amplitude-modulated quartz-enhanced photoacoustic spectroscopy," Opt. Express 24, 25943-25954 (2016).
[30] Dong, L., Kosterev, A.A., Thomazy, D., Tittel, F.K., "QEPAS spectrophones: design, optimization, and performance," Appl. Phys. B 100, 627–635 (2010).